Methodology for Standard Electromagnetic Field Measurements

NORRIS S. NAHMAN, FELLOW, IEEE, MOTOHISA KANDA, SENIOR MEMBER, IEEE, EZRA B. LARSEN, MEMBER, IEEE, AND MYRON L. CRAWFORD, SENIOR MEMBER, IEEE

Abstract—**Establishing standards for electromagnetic (EM) field measurements is a multifaceted endeavor which requires measurements made (1) in anechoic chambers, (2) at open-sites, and (3) within guided-wave structures, and the means to transfer these measurements from one situation to another. The underlying principles of these standard measurements and transfer standards fall into one of the two categories: (1) measurements and (2) theoretical modeling. In the former a parameter or a set of parameters is measured, while in the latter a parameter or set is calculated employing established physical and mathematical principles.**

In the following discussion, the three measurement topics and field transfer standards mentioned above will be discussed with the guided-wave structures being restricted to the TEM cell. Throughout the discussion the interplay between measured quantities and predicted (modeled) quantities will be seen.

The frequencies considered here range from 10 kHz to 18 GHz (and upward) and are dependent upon the physical constraints imposed by our ability to implement an actual measurement, subject to the conditions imposed by rigorous electrodynamic theory in a given analytical model.

I. Microwave Anechoic Member Measurements

MICROWAVE anechoic chambers are currently in use for a variety of indoor antenna measurements, electromagnetic interference (EMI) measurements and electromagnetic compatibility (EMC) measurements. The prime requirement is that an appropriate transmitting antenna at one location within the chamber generates a known field throughout another volume of the chamber of dimensions sufficient to perform antenna measurements. This volume is frequently referred to as a "quiet zone" and its reflectivity level will determine the performance of the anechoic chamber.

The National Bureau of Standards' (NBS) anechoic chamber is shown in a side view in Fig. 1. Pyramidal horns or open-ended waveguide (OEG) antennas are used as transmitting antennas, positioned in the access doorway with their apertures inside the plane of the absorber points on the chamber wall. The net power delivered to the transmitting antenna is the difference between the measured incident (P_{inc}) and (P_{refl}) reflected powers as measured with two directional couplers (4 ports) and is given by

$$P_{net} = P_{inc} - P_{refl} = \frac{P_1}{(1 - |\Gamma_1|^2)} \left|\frac{S_{34}}{S_{13}}\right|^2 |g(S, \Gamma)^2| - \frac{P_2}{(1 - |\Gamma_2|^2)} \frac{1}{|S_{24}|^2} |h(S, \Gamma)^2|. \quad (1)$$

Manuscript received May 24, 1985.

The authors are with the Fields Characterization Group, Electromagnetic Fields Division, National Bureau of Standards, Boulder, CO 80303.

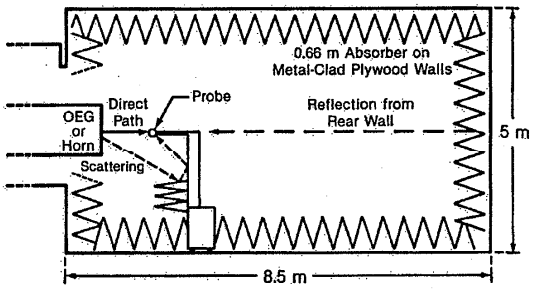

Fig. 1. Side view of the NBS anechoic chamber.

The four ports are numbered as 1 through 4, incident arm, reflected arm, source, and load, respectively. The symbols P_1 and P_2 are, respectively, power meter readings at ports 1 and 2. Γ_1 and Γ_2 represent the corresponding reflection coefficients observed looking into power meters 1 and 2. S_{ij} is a scattering parameter defined as the ratio of the complex wave amplitude emerging from port i to that incident on port j. $g(S, \Gamma)$ and $h(S, \Gamma)$ are functions of the system S-parameters and the reflection coefficients of ports 1, 2, and 4 [1].

To determine the term (S_{34}/S_{13}) and $(1/S_{24})$, NBS uses a standard mismatch and a 50-Ω matched termination. When a standard mismatch (Γ_4) is placed at port 4, the ratio of power measurements P_2 and P_1 gives

$$\frac{P_2}{P_1} = |\Gamma_4|^2 \left|\frac{S_{24}S_{34}}{S_{13}}\right|^2 \frac{1 - |\Gamma_1|^2}{1 - |\Gamma_2|^2} (1 + \Delta_1) \quad (2)$$

where $\Delta_1(S, \Gamma)$ is a complex quantity much less than unity [1]. The second step in evaluating the net power delivered to a transmitting antenna P_{net} is to replace the standard mismatch at port 4 with a well-matched power meter. The ratio of the two power measurements P_1 and P_4 is

$$\frac{P_1}{P_4} = \left|\frac{S_{13}}{S_{34}}\right|^2 \frac{1 - |\Gamma_1|^2}{1 - |\Gamma_4|^2} (1 + \Delta_2) \quad (3)$$

where Δ_2 is a complex quantity much less than unity [1]. From (2) and (3), a value for $|1/S_{24}|^2$ is obtained. In summary, two power ratio measurements are made to determine $|S_{34}/S_{13}|^2$ and $|S_{24}|^2$. The net power delivered to the transmitting antenna is then determined from two absolute power measurements P_1 and P_2, using (1).

Electromagnetic field measurements in an anechoi-

ıamber are usually performed in the near-field region of transmitting standard antenna. The approach used to es-blish the standard field involves calculating the radiated eld intensity in the near-field region of the transmitting ıtenna. The antennas now used at NBS consist of a series f open-ended waveguides at frequencies below 450 MHz ıd a series of rectangular pyramidal horns above 450 IHz.

The near zone of an open-ended, unflanged, rectangular aveguide is calculated from near-field power patterns, hich are determined from theoretically predicted far-field ɔwer patterns by use of the plane wave scattering theo-ɔm [2]. The far-field power patterns are predicted quite ɔcurately by inserting the E and H fields of the propa-ıting TE_{10} mode into the Stratton–Chu formula and in-ɔgrating over the aperture of the open-ended waveguide ɔ]. Once the far-field power pattern of an open-ended ɔctangular waveguide is determined, the plane wave scat-ɔring theory is used to predict its near-field power pattern ɔ], [5]. The near-zone gain of an open-ended rectangular aveguide is then determined by integration of the near-eld power pattern [6].

The approach used at NBS to establish a standard (cal-ılable) field at frequencies above 450 MHz involves the se of a series of rectangular pyramidal horns. In deriving ıe near-zone gain of a pyramidal horn by the Kirchhoff ıethod, Schelkunoff accounted for the effect of the horn ılare by introducing a quadratic phase error in the domi-ıant mode field along the aperture coordinates [7]. Geo-ıetrical optics and single diffraction by the aperture edges ɔields essentially the Kirchhoff results. The proximity ef-ect in the Fresnel zone can also be approximated by a ɯadratic phase error in the aperture field. To improve Schelkunoff's equation by taking into account the reflec-ıion of the diffracted fields from the horn interior and dou-ble diffraction at the aperture, the concepts of the geometrical theory of diffraction are used to determine the on-axis near-zone gain of an E-plane pyramidal horn. Tak-ing into account the preceding considerations, the im-proved near-zone gain (G) of a pyramidal horn is given by [8]

$$G = \frac{32ab}{\pi\lambda^2} R_E R_H \tag{4}$$

where R_E and R_H are gain reduction factors due to the E-plane and H-plane flares, respectively. "a" and "b" are the width (H-plane flare) and height (E-plane flare) of the rectangular horn aperture, respectively. The near-zone gain of a pyramidal horn is used to calculate the radiated field intensity in the near zone of the antenna. Fig. 2 shows typical gain reduction factors, R_E and R_H, expressed in decibels.

The failure of an anechoic chamber to provide a truly free-space test environment affects the measurement accuracies. The performance of a rectangular RF anechoic ɔhamber can be checked by measuring the relative inser-ıion loss versus separation distance between a source antenna and a receiving antenna [9].

Antenna insertion loss is the ratio of power received

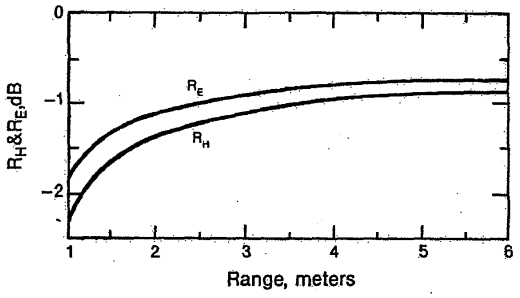

Fig. 2. Near-zone gain reduction factors, R_H and R_E, of a typical pyramidal horn at 1000 MHz.

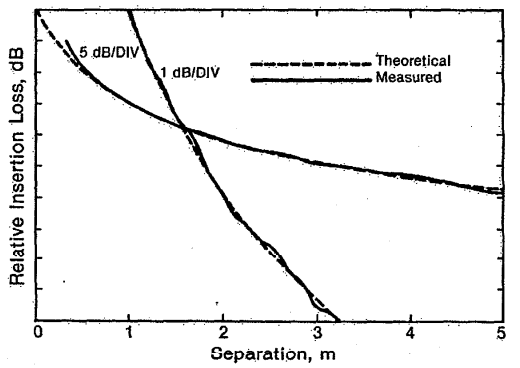

Fig. 3. Relative insertion loss between a horn antenna (main beam) and a probe, with the free-space transmission loss curve fitted at a separation distance of 1 m. Frequency = 500 MHz.

by a receiving antenna or probe to the power accepted by the transmitting antenna. If the anechoic chamber is a perfect free-space simulator, the relative insertion loss between two polarization-matched antennas varies with distance according to the Friis transmission formula as given by

$$P_r/P_t = G_r G_t(\lambda/4\pi d)^2 \tag{5}$$

where P_t is the net power delivered to the transmitting antenna, P_r is the power received by the antenna, G_t is the near-zone gain of the transmitting antenna, G_r is the near-zone gain of the receiving antenna, d is the separation distance between the two antennas in meters, and λ is the wavelength in meters. Experimental data are compared to the calculated free-space transmission loss, using appropriate near-zone transmitting antenna gains. Disagreement between the measured and calculated transmission loss is a measure of reflections from chamber surfaces. Fig. 3 shows an example of measured insertion loss compared with calculated free-space transmission loss along the axis of a horn antenna.

In the NBS anechoic chamber the largest source of error is uncertainty in the near-zone gain values of the transmitting antennas. Another source of error is uncertainty in the magnitude of multipath reflections within the anechoic chamber. Other sources of error are associated with antenna alignment, measurement of antenna separation distance, and calibration of the various instruments used. The overall worst-case uncertainty of the anechoic cham-

ber measurements (0.2–18 GHz) is the simple sum of these errors. It varies from 0.5 to 1.0 dB depending on frequency, required field level, and size of receiving antenna.

II. Open-Site Calibrations

A. General Discussion

NBS offers a calibration service for field strength meters and EMI antennas in the frequency range of 10 kHz to 1000 MHz [10], [11], [12]. The main part of a calibration consists of determining the "antenna factor" (K) which permits a receiver (RF voltmeter) to be used with the calibrated antenna to make measurements of field strength. That is, the factor (K) permits conversion of the receiver dial indication in μV or dBμV to field strength in μV/m or dBμV/m. The types of antennas involved are basically loops for H-field from 10 kHz to 50 MHz, dipoles for E-field from 25 to 1000 MHz, and monopoles for vertically polarized E-fields from 30 kHz to 300 MHz.

There are two independent techniques by which field strength can be evaluated. These are called (1) the "standard field" method and (2) the "standard antenna" method. The former consists of generating and calculating a desired component of standard field in terms of the type and dimensions of a transmitting antenna, its current distribution or net delivered power, the distance from the transmitting antenna to the field point, and the effect of ground reflections (if present). The second method consists of generating an unknown field, but measuring it with a calculable receiving antenna. The voltage or current induced in a standard antenna by the component of field being evaluated is measured. The field strength value is then calculated in terms of this induced voltage, the dimensions and form of the receiving antenna, and its orientation with respect to the field vector.

At frequencies below about 50 MHz for loop antennas, a quasistatic near-zone magnetic field is produced by a balanced single-turn transmitting loop of 10-cm radius. Above 25 MHz for dipole-type antennas, a radiated far-zone electric field is produced and evaluated in terms of the open-circuit voltage induced in a self-resonant receiving dipole. Between 30 kHz and 300 MHz for vertical monopoles and small probes, an elliptically polarized electromagnetic field is produced by a transmitting monopole above a 30 × 60 m conducting ground screen. The instrumentation used by NBS and the uncertainties for these calibrations are discussed in the following four sections. All the techniques described here for field strength standards are applicable only for steady-state RF fields with sinusoidal time variation. They are not intended for use with pulsed fields or other broad-band applications.

B. Standards for Field Strength Meters, 10 kHz to 10 GHz (Tunable RF Voltmeter)

For most field strength meters, the first part of a calibration is checking the receiver as a tunable RF voltmeter [13], [14]. This generally includes measurement of "linearity" (dial indication versus input level) and checking the internal step attenuators at several frequencies [12]. A summary of these tests is given in the following list:

Type of NBS Measurement	Frequency range	Amplitude range	Calibration uncertainty
1) Receiver indication as a function of signal frequency, at a few voltage levels.	10 kHz–400 MHz 400–1000 MHz 1–10 GHz	1 μV–10 mV 10 μV–10 mV 100 μV–100 mV	±1/2 dB ± 3/4 dB ± 1 dB
2) Attenuation of the step attenuators at a few frequencies.	10 kHz–1 GHz 1–10 GHz	(0–80 dB) (0–80 dB)	± 1/4 dB ± 1/2 dB
3) Receiver linearity, which is independent of frequency.	10 kHz–1 GHz 1–10 GHz	10 μV–100 mV 10 μV–100 mV	± 1/4 dB ± 1/2 dB

C. Magnetic Field Strength Standards for Loops, 10 kHz to 50 MHz (Standard Field Method)

The response of an electrically small receiving loop antenna is proportional to the average normal component of magnetic field strength incident on the antenna. At NBS a calculable quasistatic magnetic field is produced for calibrating these antennas, using a circular single-turn balanced transmitting loop. The current in this loop of 10-cm radius is approximately constant in amplitude and phase around the loop.

The receiving loop antenna being calibrated is positioned on the same axis as the transmitting loop at a distance of 1.5–3 m. Fig. 4 shows the NBS calibration setup. The normal component of the magnetic field, averaged over the area of the receiving loop, is given by [15]

$$H \cong \frac{Ir_1^2}{2R_0^3}\left[1 + \left(\frac{15}{8}\right)\left(\frac{r_1 r_2}{R_0^2}\right)^2\right]\sqrt{1 + \beta^2 R_0^2} \qquad (6)$$

where

H rms value of the magnetic field, A/m,
I rms current in the transmitting loop, A,
r_1 radius of the transmitting loop, m,
r_2 radius of the receiving loop, m,
R_0 $\sqrt{d^2 + r_1^2 + r_2^2}$,
d axial distance between the two loops, m,
β $2\pi/\lambda$, and
λ free-space wavelength, m.

The current in the transmitting loop is measured with a vacuum thermocouple calibrated with direct current. It is at the top of the loop winding, as shown in Fig. 4, and its dc output is measured with a millivoltmeter. The RF/dc

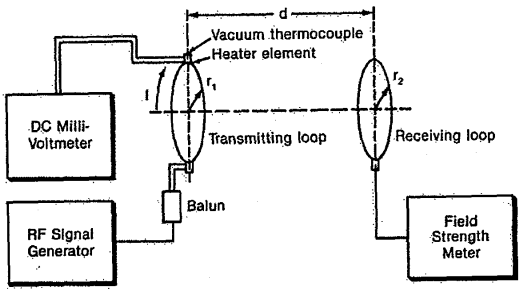

Fig. 4. Diagram of the NBS measurement system for calibrating loop antennas.

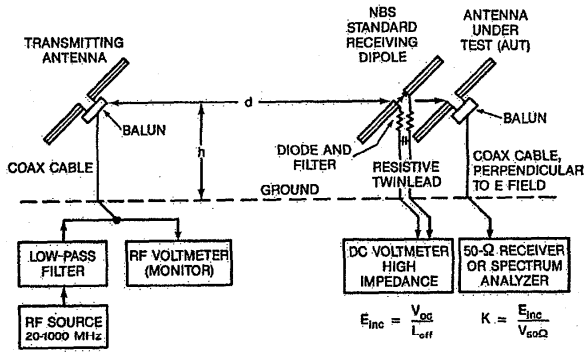

Fig. 5. Field site instrumentation for calibrating horizontal dipoles, 25–1000 MHz.

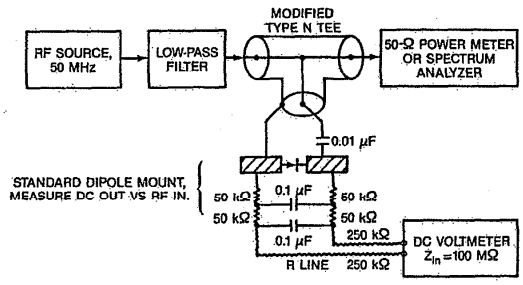

Fig. 6. Instrumentation for measuring V_{oc} versus V_{dc} of the NBS standard dipole.

substitution error of the thermocouple is <1 percent at frequencies up to 50 MHz. Equation (6) is accurate within ± 0.2 percent if $\beta R_0 \leq 1$ and $r_1 r_2 / R_0^2 \leq 1/16$. At higher frequencies the correction term under the radical becomes appreciable for the usual spacing of 1.5–3 m used at NBS. The uncertainty of calibrating loop antenna factors NBS is $\pm 1/4$ dB for frequencies up to 5 MHz, $\pm 1/2$ dB between 5 and 30 MHz, and ± 1 dB between 30 and 50 MHz.

While coaxial loops are normally used for calibration purposes, the two loops can also be positioned in the same plane. Co-planar loops are advantageous under certain conditions, e.g., with some ferrite core antennas in which the core length is large. In this case, the calibrating value of H is half of that given by (6).

The calibration and subsequent measurement of magnetic field strength (H) are often expressed in terms of the electric field (E) that would exist if the measurement were made in free space, in which case $E/H \cong 377\ \Omega$. When such a field strength meter is used to make measurements near the ground, the indicated value of electric field is not necessarily valid. The same is true for measurements made in the near zone of a transmitting antenna. However, the value of the magnetic component (H) can still be measured correctly.

For calibrating loops or H-field probes at a higher field level, it is possible to use the calculable H-field generated in a TEM cell or at the center of a flat multiturn coil, or at the midpoint of a Helmholtz coil pair.

D. Electric Field Strength Standards for Dipoles, 25–1000 MHz. (Standard Antenna Method) [10], [16].

1) Definition of E_{inc}: The magnitude of the electric field component at a given point in a locally generated field is determined at NBS from the open-circuit voltage (V_{oc}) induced in a standard (calculable) half-wave receiving dipole. The field site instrumentation is shown in Fig. 5. The induced voltage is measured across the center gap of the dipole, which is oriented horizontally and parallel to the E vector of the incident field. In using the standard antenna method, a plane-wave field is generated by a suitable transmitting antenna, such as a log periodic or half-wave dipole. The magnitude of this incident field is measured with the standard dipole by the relation

$$E_{inc} = \frac{V_{oc}}{L_{eff}} \tag{7}$$

where

E_{inc} field strength of the locally generated field, V/m,
V_{oc} open-circuit voltage induced in the standard dipole, V
L_{eff} effective length of the standard dipole, m.

2) Measurement of V_{oc}: The RF voltage picked up by the $\lambda/2$ standard dipole (V_{oc}) is measured in terms of the rectified dc voltage, as detected by a high-impedance Schottky diode connected in shunt across the center gap of the antenna. The diode output is filtered by a balanced RC network and this dc voltage is measured with a high-impedance dc voltmeter. As shown in Fig. 6, the RF/dc substitution of the detector network in the standard dipole is determined by applying a known RF voltage at 50 MHz across the standard dipole gap. The antenna rods making up the standard dipole are removed for this measurement.

The high impedance of the diode "voltmeter" eliminates the necessity for a separate measurement of the dipole impedance, since the source impedance of a resonant dipole is low compared with that of the voltmeter. Another advantage of this approach is that the measurement of E_{inc} is not affected appreciably by the presence of ground or other perturbing objects. However, a subsequent measurement of field strength by the calibrated customer dipole will be affected by ground due to impedance change of the customer's dipole, which is loaded with a 50-Ω receiver. Also, the standard dipole used to measure E_{inc} lacks frequency selectivity, so it is not possible to perform the NBS calibration in the presence of strong interfering signals.

The range of filtered dc output voltage used at NBS is normally 0.5–1.5 V, which is generally sufficient to avoid calibration uncertainty caused by ambient fields and temperature changes of the diode detector. The response of the diode "voltmeter" is independent of frequency up to about 500 MHz, with slightly increased response above this frequency due to the approaching series-resonant frequency of the diode mount.

3) Determining L_{eff} of the Standard Dipole: The effective length of a receiving dipole is a measure of the E-field intercept length, analogous to the effective area of an aperture antenna. L_{eff} is derived in terms of the current distribution along the length of a *transmitting* dipole. The reciprocity theorem is invoked in order to use the same value of L_{eff} for a receiving dipole. It could be noted that L_{eff} cannot be defined in terms of the current distribution on a receiving dipole. By definition, the effective length of a transmitting dipole with a physical length L and input current I_0 is given by

$$L_{eff} = \frac{\text{Moment of dipole current distribution}}{\text{Input current at the feed point (center) of the dipole}} = \frac{1}{I_0}\int_{-L/2}^{+L/2} I(l)\, dl. \tag{8}$$

Assuming a cosinusoidal current distribution on an infinitesimally thin dipole, the effective length of a half-wave dipole in free space is

$$L_{eff} = \frac{\lambda}{\pi}. \tag{9}$$

However, the current distribution on a real dipole (in its transmitting mode) is not exactly cosinusoidal. An approximate solution for the current distribution on a cylindrical transmitting dipole was derived by Schelkunoff [17], [18] and this solution is used for calculating L_{eff} of the NBS standard dipole. Also, in order to achieve self resonance of the dipole (zero reactance) it is necessary to make its length slightly shorter than $\lambda/2$. The required length for resonance as derived by Schelkunoff depends on the dipole length-to-diameter ratio, and is

$$\text{Required } L = \left(\frac{\lambda}{2}\right)\left[1 - \frac{0.2257}{\ln(\lambda/D) - 1}\right] \tag{10}$$

where D is the diameter of the standard dipole, m.

If a $\lambda/2$ dipole is shortened slightly to obtain zero reactance, the theoretical resistance ($R_{in} = Z_{in}$) depends on the length-to-diameter ratio (L/D) as follows:

L/D ratio	L/λ at resonance	Dipole R_{in}
100	0.46	55 Ω
1000	0.48	65 Ω
100 000	0.49	70 Ω

The standard dipole sets used for field strength calibration at NBS are made of cylindrical metal tubes which are 3–5 percent shorter than the free-space $\lambda/2$ depending on the L/D ratio. It is possible to use these dipoles at the resonant frequencies and calculate L_{eff} from (9). The effective length of a thin nonresonant dipole at frequencies up to at least the first resonance is given approximately by

$$L_{eff} = \left(\frac{\lambda}{\pi}\right)\left[\tan\left(\frac{\pi L}{2\lambda}\right)\right]\left[\cot\left(\frac{\pi}{4}\right) \cdot \left(1 - \frac{0.2257}{\ln(2L/D) - 1}\right)\right]. \tag{11}$$

For signal frequencies well below self resonance, the receiving dipole (probe) is electrically short and the effective length approaches a value equal to half the physical length. However, the impedance of an electrically short dipole is a high capacitive reactance, and it is difficult to fabricate an "open-circuit" dipole whose load impedance is high compared with the source impedance of a short dipole. In this case, the voltage dividing ratio between the source and load impedance is uncertain, and the short dipole can be used only as a transfer probe, but not as a standard (calculable) receiving antenna. (See Section V of this paper for a discussion of the theory and use of transfer probes.) Note that a transfer probe (E or H field) can be used to measure an unknown field, but only after it has been calibrated in a standard field, such as that of a TEM cell. (See Section IV of this paper for a discussion of TEM cells.)

As indicated in Fig. 5, the "antenna factor" (K) of a customer's antenna or other antenna under test (AUT) is determined by placing it in the same field (same position) just measured with the resonant standard receiving dipole, and using the relation

$$K = \frac{E_{inc}}{V_{50\Omega}}$$

or

$$K_{dB} = 20 \log (E_{inc}) - 20 \log (V_{50\Omega}) \tag{12}$$

where

E_{inc} magnitude of the standard calibrating field, V/m,
$V_{50\Omega}$ voltage produced by the AUT across a 50-Ω load, V.

K is a transfer function which is related, in a reciprocal fashion, to the antenna gain. However, unlike antenna gain, the impedance mismatch between the antenna and its load (50-Ω receiver) is included in the value of K. Fig. 7 is a graph of the theoretically expected antenna factor for a thin $\lambda/2$ dipole. K is most often expressed in decibels, as follows:

$$K_{dB} = E_{inc_{dB/\mu V/m}} - V_{50\Omega_{dB\mu V}}. \tag{13}$$

In this form, K is a dimensionless ratio given in terms of the known incident E-field with respect to 1 μV/m, and the antenna response across a 50-Ω load with respect to 1 μV.

4) Using the Calibrated AUT: An unknown E-field can be determined with the calibrated antenna (AUT) in terms

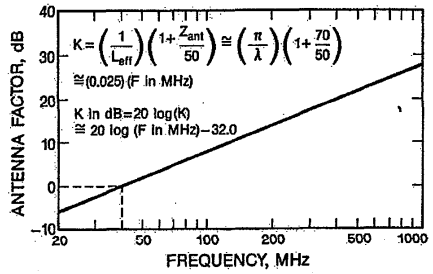

Fig. 7. Theoretically expected antenna factor of a thin λ/2 dipole and 50-Ω receiver, excluding cable loss and balun loss.

of the measured pickup voltage at the 50-Ω receiver, using the equation

$$E = (K)\ (V_{50\Omega}) \tag{14a}$$

where

E strength of the field being measured, V/m,
K antenna factor from the calibration data, at the given frequency,
$V_{50\Omega}$ pickup voltage as measured with the 50-Ω receiver

or

$$E_{\mathrm{db}\mu\mathrm{V/m}} = V_{50\Omega_{\mathrm{dB}\mu\mathrm{V}}} - K_{\mathrm{dB}}. \tag{14b}$$

It could be noted that the customer's receiver, with attached antenna, can also be calibrated as a system to measure the field strength directly.

A field strength measurement made with the calibrated AUT may be in error if it is made at a lower antenna height than that used during the calibration (about 3 m), or if the electrical ground contants at the measuring site are appreciably different from those at the calibrating site [10]. This results from a change in input impedance of the customer's antenna due to the proximity of the ground. A change of impedance doesn't affect the measurement of V_{oc} by the open-circuit standard dipole, but it changes the mismatch between the customer's antenna and a 50-Ω receiver. However, if the customer's antenna is calibrated at a height greater than 2λ, the calibration results in essentially a free-space value. The error is generally less than 10 percent for heights greater than 0.5λ. The error would also decrease if the antenna load impedance (receiver input impedance) were high, and would approach zero as the load impedance approaches infinity. Also, if the receiver had a sufficiently large value of input impedance, the calibration would be independent of the antenna polarization and properties of the ground. Fig. 8 is a graph of the impedance of a typical dipole as a function of length or signal frequency, and Fig. 9 is a graph of the impedance of a typical loop for comparison.

NBS usually determines dipole antenna factors at an outdoor site, generally using a 30 × 60 m ground screen site which is provided with an air-inflated all-weather cover. Dipole calibrations can also be performed in the anechoic chamber for frequencies above 200 MHz, using

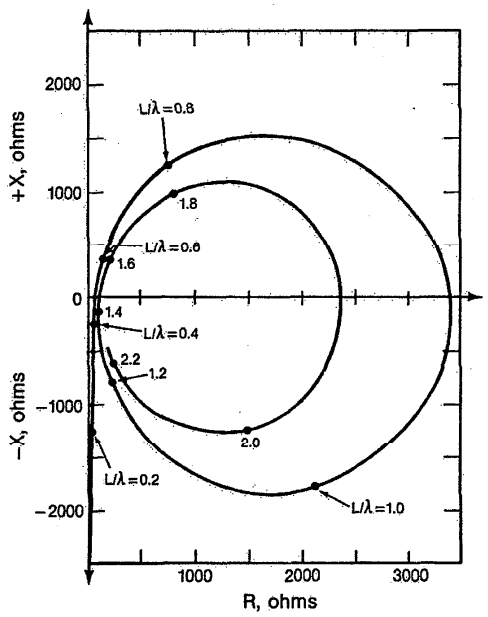

Fig. 8. Free-space impedance of a dipole antenna, length/diameter ratio = 2000.

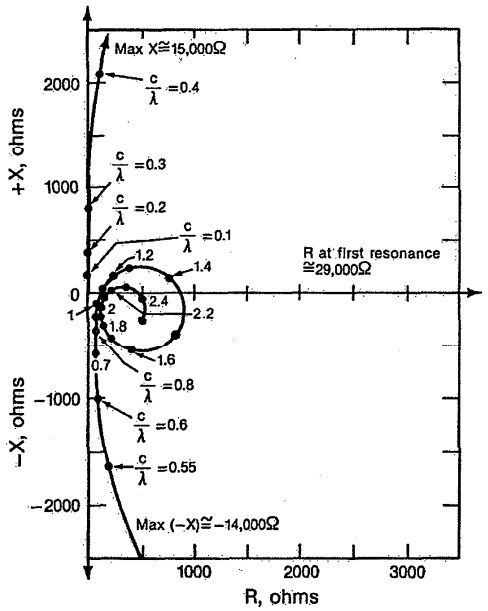

Fig. 9. Free-space impedance of a loop antenna, circumference/wire diameter = 200.

the standard-field approach discussed in Section II of this report. The calibration uncertainty at the present time for either facility is ±1 dB.

E. Electric Field Strength Standards for Vertical Monopoles, 30 kHz to 300 MHz (Standard Field Method).

After considering several approaches for generating a standard (calculable) field to calibrate vertically polarized

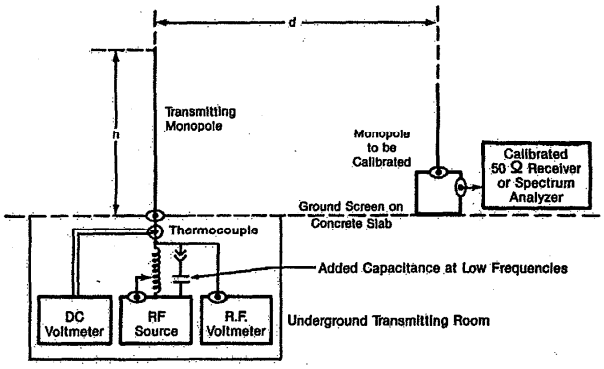

Fig. 10. Field site instrumentation for calibrating monopole antenna factors.

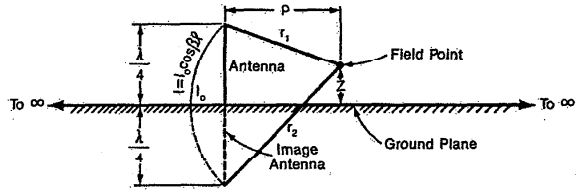

Fig. 11. Geometry for the EM field of a thin λ/4 transmitting monopole antenna.

antennas, the system chosen at NBS consists of a thin cylindrical transmitting monopole over a 30 × 60 m metallic ground plane. The field strength is calculated in terms of the magnitude and distribution of the monopole current and other factors such as: (1) monopole height, (2) horizontal distance from the transmitting antenna to the field point, (3) vertical height of this point above the ground plane, and (4) electrical conductivity of the ground system.

The basic arrangement of the NBS standard-field system is shown in Fig. 10. The height of the transmitting monopole is adjustable, with a maximum height of about 3 m. The electrical height of this antenna is λ/4 (resonant) at 25 MHz, but only 0.0003 λ at 30 kHz. At frequencies above 25 MHz, the antenna height is reduced to a λ/4 value. The base diameter of the monopole used is about 1 cm. The monopole is excited through a coaxial cable from the transmitting room located beneath the concrete ground slab.

Equations (16), (17), and (18) give the magnitudes of the three field components E_z, E_ρ, and H_ϕ of a transmitting λ/4 monopole above a perfect ground plane of infinite extent. The geometry for these field components is shown in Fig. 11.

$$E_z = 30\, I_0 \left(\frac{e^{-j\beta r_1}}{r_1} + \frac{e^{-j\beta r_2}}{r_2}\right) \tag{16}$$

$$E_\rho = \frac{30\, I_0}{\rho}\left[\left(\frac{e^{-j\beta r_1}}{r_1}\right)\left(z - \frac{\lambda}{4}\right) + \left(\frac{e^{-j\beta r_2}}{r_2}\right)\left(z + \frac{\lambda}{4}\right)\right] \tag{17}$$

$$H_\phi = \frac{I_0}{4\pi\rho}\left(e^{-j\beta r_1} + e^{-j\beta r_2}\right) \tag{18}$$

where

E_z	vertical E component, V/m,
E_ρ	horizontal E component, V/m,
H_ϕ	magnetic (H) field, encircling the monopole, A/m,
I_0	RMS base current of the monopole, A,
β	$2\pi/\lambda$ = the wavelength constant, and
z, ρ, r_1, and r_2	distances to the field points, m.

For frequencies near self resonance, the monopole base current is measured with an RF ammeter consisting of a thermoconverter which has been calibrated with known values of dc current. At lower frequencies where the monopole input impedance (Z_{in}) is a high-capacitive reactance, the base current is calculated from Ohms law in terms of the base voltage measured with a vacuum-tube voltmeter and the theoretical input impedance. At very low frequencies, Z_{in} may be calculated from the antenna capacitive reactance, using Schelkunoff's equation in [18]:

$$C_a = \frac{55.63\, h}{\ln\,(h/a) - 1} = 30.9 \text{ pF}$$

for a 3 m monopole 1 cm in diameter (19)

where

C_a	monopole input capacitance, pF,
h	monopole height, m,
a	monopole radius, m.

The standard field equations are relatively simple for the case of a ground plane with infinite extent and infinite conductivity. However, the current on a vertical monopole with finite diameter departs from the sinusoidal current distribution of a filamentary monopole. This does not seriously affect the calculated values of current-related field components, such as the magnetic field or the far-zone electric fields. But the low-frequency near-zone quasi-static, electric-field components are more nearly *charge* related and are given by the spatial derivative of the current distribution. Hence, there is greater uncertainty in calculating the E-field components at frequencies well below that of a λ/4 resonant monopole.

Examples of calculated standard-field data are shown in Fig. 12 for a 3-m monopole operating at a frequency of 25 MHz, for which the electrical length is λ/4. The base current used in this case is 1 A. Vertical and horizontal components of the electric field are plotted versus horizontal distance from the antenna, for a height 1.2 m above the ground plane. Similar curves are shown in Fig. 13 for the same antenna at a frequency of 200 kHz, which correspond to the near-zone case.

If a transmitting monopole is electrically short, that is, if the height is less than λ/4 and the frequency is below resonance, the current distribution is triangular. The field equations are more complicated than the three given above

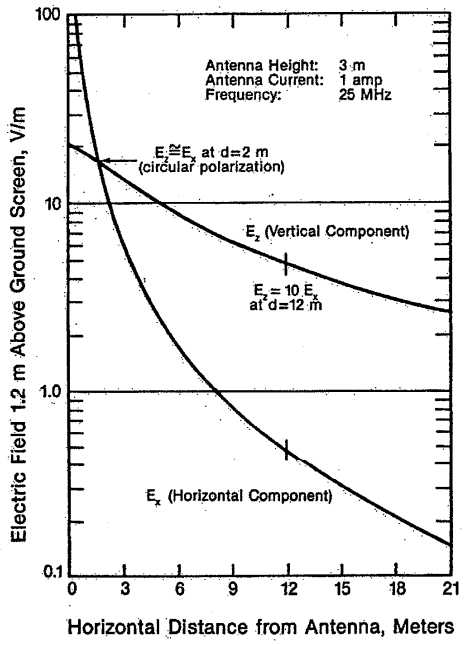

Fig. 12. Theoretical electric field of a λ/4 transmitting monopole.

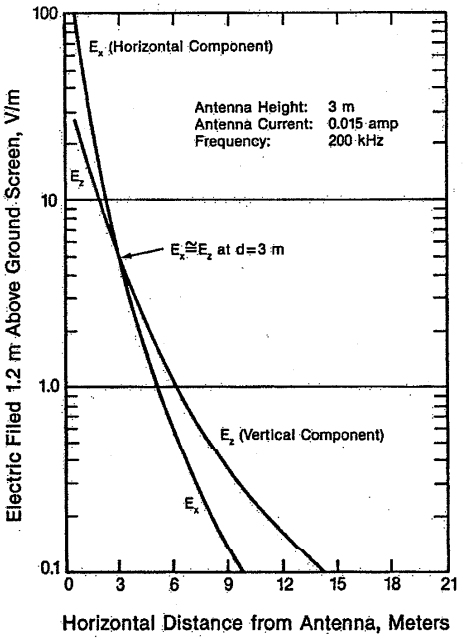

Fig. 13. Theoretical electric field of a 0.002 λ transmitting monopole.

and are not included here, but can easily be programmed [19]. It could be noted that the EM field values in the half space above ground are the same as those in each half volume of a center-fed λ/2 dipole in free space. The input impedance of a monopole above perfect ground is half that of a dipole in free space. The power required to generate a given field strength is half that required for a dipole, but the radiated power goes into half the volume, so the field is the same. Measurements of Z_{in} at the NBS ground screen facility with a commercial impedance meter were performed to check the theoretical values from 0.5 to 50 MHz. Measurements of the monopole capacitance were made at lower frequencies with a commercial Q meter. Also, checks have been made of the calculated E-field versus measurements with a small active calibrated field-strength probe. The agreement found between the various techniques was within 1 dB at all frequencies checked.

A metal ground plane having a thickness of several skin depths, so that the ground currents will not penetrate through, exhibits essentially infinite conductivity for the frequency range covered here. The horizontal dimensions of the NBS ground screen (about 30 × 60 m) are several times the height of the monopole used (up to 3 m) in order to minimize the effect of wave reflections from the edges of the plane. At low frequencies, where the ground screen is electrically small, it is difficult to achieve capacitive coupling to the reinforced concrete slab or to the surrounding earth, even though the underground transmitting room has a large ground rod. Therefore, further experimental testing is required of field uniformity versus azimuth angle, and field strength reduction versus distance from the transmitting antenna point.

To summarize the calibration and use of a customer's monopole, the antenna factor (K) of the AUT is determined by immersing it in a calculated vertically-polarized field (E_z) about 20 m from the NBS transmitting monopole. A coax cable is usually attached to and considered part of the antenna when calibrating (K). The equation used to determine (K) is the same as that for dipole calibrations, namely

$$K = \frac{E_{\text{inc}}}{V_{50\Omega}} \tag{20a}$$

or

$$K_{\text{dB}} = E_{\text{inc}_{\text{dB}\mu\text{V/m}}} - V_{50\Omega_{\text{dB}\mu\text{V}}}. \tag{20b}$$

The theoretically expected antenna factor of an electrically short monopole above a perfect ground is given by

$$K = \left(\frac{1}{h_{\text{eff}}}\right)\left(1 + \frac{Z_a}{50}\right) \tag{21}$$

where

h_{eff} effective height of the receiving monopole, m, and
Z_a monopole input impedance.

For example, for a 1-m whip of 0.5-cm diam at frequencies below 10 MHz, $h_{\text{eff}} \cong 0.5$ m, and $C_a \cong 11$ pF. In this case $Z_a \cong -j(14470/\text{F, MHz})$ and $K \cong 579/\text{F, MHz}$.

It can be seen that the antenna factor of a short monopole (or dipole) is inversely proportional to frequency, while the antenna factor of a resonant monopole (or dipole) is directly proportional to frequency.

An unknown field strength (E) can be determined with a calibrated monopole by measuring its output voltage with

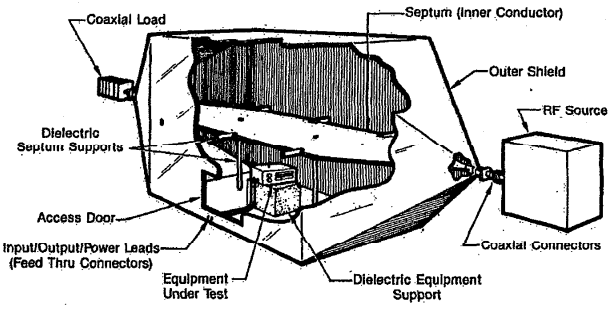

Fig. 14. Isometric view of a TEM cell for establishing standard EM fields.

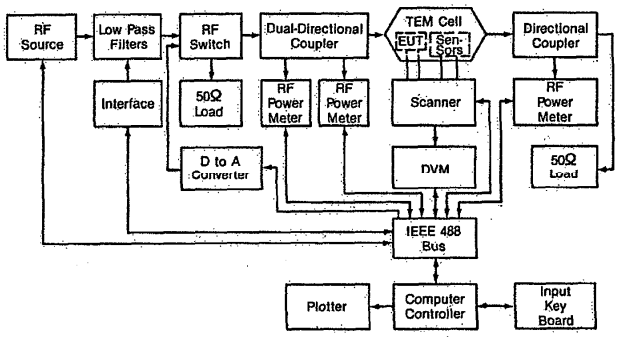

Fig. 15. Block diagram of an automated TEM cell system for establishing known EM fields.

a 50-Ω receiver or spectrum analyzer, using the equation

$$E_{\mu V/m} = (K)(V_{50\Omega}) \tag{22a}$$

or

$$E_{dB\mu V/m} = V_{50\Omega_{dB\mu V}} + K_{dB}. \tag{22b}$$

The calibration of monopole antenna factors at NBS is performed at the outdoor ground-screen site for frequencies from 30 kHz to 300 MHz with an uncertainty of ±1 dB. For frequencies up to 10 MHz and for monopoles or probes having a height less than 0.5 m, these calibrations can also be performed in a large TEM cell, with the same uncertainty.

III. Generating Standard EM Fields Using a TEM Cell

Transverse electromagnetic (TEM) transmission line cells are devices used for establishing standard electromagnetic (EM) fields in a shielded environment [20], [21], [22]. Their application is becoming increasingly widespread because of their versatility, measurement accuracy, and ease of operation.

A TEM cell is essentially a 50-Ω triplate transmission line with the sides closed in to prevent radiation of RF energy into the environment and to provide electrical isolation. A properly designed cell, terminated in its characteristic impedance, is capable of producing a calculable *E*- and *H*-field for calibrating an electrically small antenna or RF probe. An isometric view of a cell as used for establishing standard EM fields is shown in Fig. 14. Fig. 15 is a block diagram of an automated TEM cell system. The cell consists of a section of rectangular coaxial transmission line tapered at each end to adapt to standard coaxial connectors. The line and tapered transitions are designed to have a nominal characteristic impedance of 50 Ω along their length to ensure minimum voltage standing wave ratio. A fairly uniform EM field is established between the plates inside the cell when RF energy is conducted in the line from a transmitter connected to the cell's input port. A 50-Ω termination is connected to the cell's output port. The expression for determining the electric field E in volts/meter in the cell is given by

$$E = \frac{V}{b} = \frac{\sqrt{PZ_o}}{b} \tag{23}$$

where

- V rms voltage on the septum (center conductor),
- b separation distance between the septum and lower or upper walls, m,
- P net power flow to the cell, W,
- Z_o real part of the cell's characteristic impedance ≅ 50 Ω.

The wave traveling through the cell has essentially a free-space impedance (377 Ω), thus providing a close approximation to a far-field plane wave propagating in free-space. The design of TEM cells can be based on an approximate equation for the characteristic impedance of a rectangular transmission line [23]

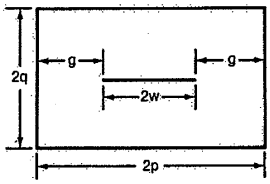

Fig. 16. Block diagram of an automated TEM cell system for establishing known EM fields.

$$Z_o \simeq \frac{377}{4\left[\frac{p}{q} - \frac{2}{\pi}\ln\left(\sinh\frac{\pi g}{2q}\right)\right] - \frac{\Delta c}{\epsilon_0}} \tag{24}$$

where p, q, and g are shown in Fig. 16, and $\Delta c/\epsilon_0$ is related to the fringing capacitance between the edges of the septum and the side walls. For large gaps ($g/p > 0.2$) this fringing term approaches zero [24].

The detailed electric field distribution inside the cell can be found approximately using Jacobian elliptic functions [23]. A tabulation of the electric field distribution inside cells with two different cross sections (typical of commercially available cells) is given in [25].

The upper useful frequency for a cell is limited by distortion in the test field caused by multimoding and resonances that occur within the cell at frequencies above the cell's multimode cut-off. Resonant frequencies, f_{res}, associated with these modes can be found from the expression [26]–[28]

$$F_{res} = \sqrt{f_{mn}^2 + \left(\frac{vl}{2L}\right)^2} \tag{25}$$

where f_{mn} are the frequencies of the higher order mode(s) excited inside the cell, v is the wave propagation velocity ($\cong 3.0 \times 10^8$ m/s), L is the resonant length of the cell in meters, and l, m, and n are integers corresponding to multiples of the resonant length and the particular waveguide mode. It is important to note: (1) the influence of the first-order TE modes does not become significant until approaching their resonances, and (2) since most cells are designed with the center plate (system) centered symmetrically, the odd-order TE modes are not excited in an empty cell. The presence, however, of a device placed in the cell will excite these modes in varying degrees depending on size, shape, and placement location.

The estimated measurement uncertainty in establishing EM fields in a TEM cell operating in the fundamental (TEM) mode ranges from ± 0.5 dB to ± 2 dB depending on the shape of the cell (width to height ratio) and the quality of design.

The main limitation of TEM cells is the size versus upper useful frequency range. The major design considerations are:

1) maximize the usable test cross section area;
2) maximize the upper useful frequency range;
3) minimize the cell impedance mismatch or voltage standing wave;
4) maximize the uniformity of EM field pattern characteristics of the cell.

It is important that the size of the AUT to be tested does not exceed approximately one-third of the smallest linear dimension of the cell [29], [30]. This is because the device tends to short out the test field in the region it occupies between the plates, increasing the amplitude of the electric field. This error can be partially corrected by using a procedure described in [25] or by measuring the field strength in the region above and below the device under test with miniature E-field probes and then making appropriate corrections.

IV. Electric and Magnetic Field Probes as Transfer Standards

The term "transfer standard," as used here, refers to an electrically small antenna or RF probe. This can be a short dipole for sensing E-fields or a small loop for H-fields, which has a known response over a given and relatively small range of frequency or amplitude. Such an antenna can be used to measure or verify the field strength as a function of frequency, for example, in an anechoic chamber. This check is especially useful if the transfer standard has been calibrated by an independent approach over the same frequency range. A transfer probe can also be used to check the field level as a function of distance from the transmitting antenna, such as in an anechoic chamber. One method used at NBS is to adjust (and measure) the power delivered to the transmitting antenna until the probe output reaches a given (constant) indication. In this way the field strength also remains constant, since the frequency and probe response are maintained constant, and the transmitting power required to obtain this (constant) response is recorded as a function of separation distance between the transmitting antenna and receiving probe. Then, from the required transmitting power, the (near-zone) gain reduction of the antenna—or the "ripple" in field strength due to reflections inside the anechoic chamber—can be evaluated.

NBS is engaged in the design of electric and magnetic field RF probes. The work involves both theoretical and experimental aspects of quantifying EM fields, including the fabrication and calibration of electric and magnetic probes.

Since most electric field RF probes consist of three electrically short, mutually orthoganol dipole antennas with three diode detectors, we review the characteristics of an electrically short dipole with a nonlinear load (dipole detector) as shown in Fig. 17. The induced open-circuit voltage at the dipole terminal is given by

$$V_{0c} = E_{inc} L_{eff} \tag{26}$$

where E_{inc} is the normal incident electric field strength and L_{eff} is the effective length of the dipole. For an electrically short dipole, the effective length L_{eff} and driving point capacitance C_a are approximately

$$L_{eff} = \frac{L(\Omega - 1)}{(\Omega - 2 + \ln 4)} \tag{27}$$

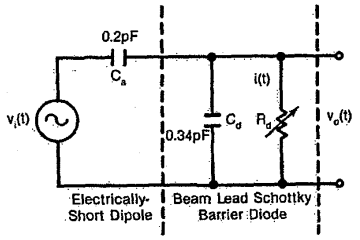

Fig. 17. Thevenin's equivalent circuit of an electrically short dipole with a shunt diode detector.

and

$$C_a = \frac{4\pi\epsilon_0 L}{(\Omega - 2 - \ln 4)} \tag{28}$$

where L is the physical length of the dipole antenna in meters, ϵ_0 is the free-space permittivity in farads/meter, Ω is the antenna thickness factor ($\Omega = 2 \ln (L/a)$), and a is the antenna radius in meters.

Solving a first-order nonlinear differential equation associated with the Thevenin's equivalent nonlinear circuit shown in Fig. 17 for the detected dc voltage V_o, one can show [31]

$$V_o = -\frac{\alpha}{4}\left(\frac{V_i}{1 + C_d/C_a}\right)^2 \tag{29}$$

where α is derived from the diode characteristics (about 38 V^{-1}) and for large V_i

$$V_o \cong -\frac{V_i}{1 + C_d/C_a}. \tag{30}$$

Equation (29) indicates that for a small induced RF voltage V_i, the output dc voltage V_o is a square-law function of the induced voltage. On the other hand (30) indicates that for a large induced voltage V_i, the output dc voltage V_o is directly proportional to the induced voltage. The linear and square-law regions of the detected output voltage can be seen by examination of Fig. 18.

A broad-band electric field RF probe was developed at NBS for the frequency range of 200 kHz to 1000 MHz [32]. This isotropic antenna unit consists of three mutually orthogonal dipoles, each 5-cm long, with beam-lead Schottky-barrier diode detectors, and high-resistance plastic twinleads. Fig. 18 gives the detected dc output voltage as a function of field strength from 1 to 1000 V/m. Fig. 19 shows the typical frequency response of this electric field RF probe.

For magnetic field measurements, NBS has analyzed various basic design considerations for broad-band magnetic field probes [33]. Three configurations are discussed in this present paper, namely: (1) a short-circuit current loop, (2) an open-circuit voltage loop, and (3) a compensated open-circuit voltage loop. To make the response of a loop antenna flat over the frequency range of interest, the Q of the loop antenna is reduced by means of a loading resistor.

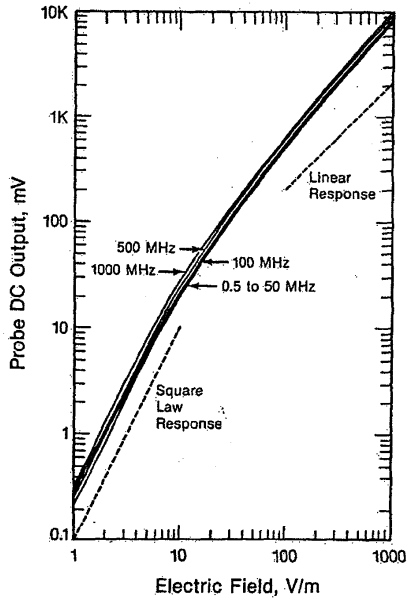

Fig. 18. Typical detected output of an EFM-5 dipole as a function of field strength, at several frequencies.

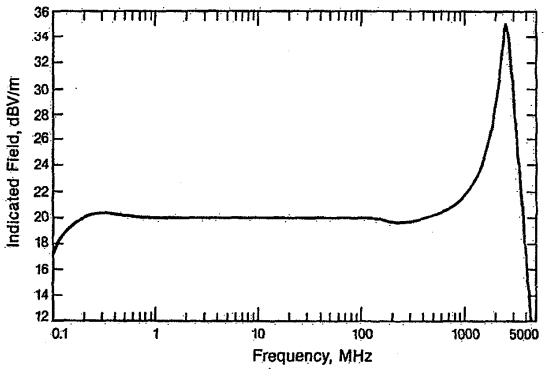

Fig. 19. Typical response of an EFM-5 monitor versus frequency, at a field strength of 20 dBV/m (10 V/m).

This NBS isotropic magnetic field probe (MFM-10) was developed using a compensated open-circuit voltage loop configuration to achieve a flat frequency response from 300 kHz to 100 MHz. The configuration of a compensated open-circuit voltage loop and its equivalent circuit are shown in Fig. 20. In this configuration a series RC circuit is added across the diode detector in order to: (1) lower the Q of the loop, and (2) shift its resonance to a lower frequency.

To gain some physical insight into a compensated open-circuit loop, consider a 5-turn loop with a 10-cm diam in which a resistor R is added across the diode detector as shown in Fig. 20. First, without this shunt resistor R, the sharp resonance of the loop is observed at about 23 MHz. Since the inductance of a 5-turn loop with a 10-cm diam is about 7 μH, and the loop and diode detector have a

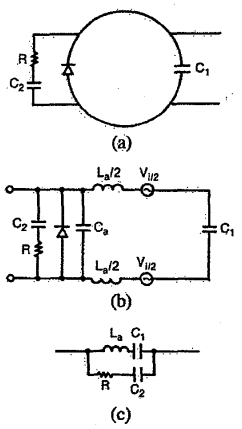

Fig. 20. (a) Compensated open-circuit voltage-loop antenna. (b) and (c) Equivalent circuits.

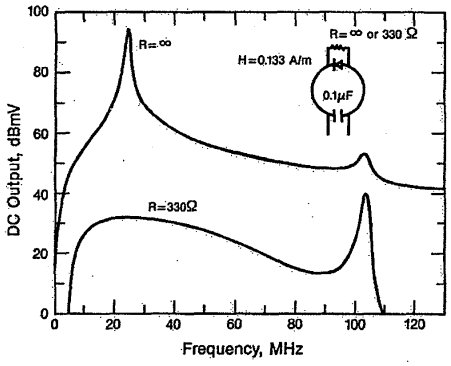

Fig. 21. Response of a compensated open-circuit-voltage loop antenna (5-turn 10-cm diam).

parallel capacitance of 6 pF, the loop resonance of about 23 MHz is predictable. There are also higher resonances, the lowest of which at 102 MHz is due to the loop inductance and loop capacitance, or equivalently, these resonances occur when the total length of the multiturn loop is approximately equal to $\lambda/2$ or one of its multiples. Thus in this configuration, we observed two distinct resonances. To achieve a "flat" loop response, a shunt resistance, R was added across the diode detector. Fig. 21 indicates this phenomenon, after a 330-Ω resistor was added across the diode detector. As expected, the resonance frequencies are not shifted by this compensation.

To further improve the "flatness" of the loop response, the shunt resistance R needs to be further reduced. At the same time, to shift the lowest resonance to the design goal of 100 kHz, the external capacitor C_2 in series with resistor R is added across the diode detector, as illustrated in Fig. 20. The capacitor C_2 also serves as a dc block.

For the purpose of determining the resonant frequencies of the compensated open-circuit voltage loop, its equivalent circuit given in Fig. 20(b) can be simplified as shown in Fig. 20(c), since the loop capacitance and diode capacitance are much smaller than the external capacitors C_1 (0.1 μF) and C_2 (0.1 μF), and can thus be ignored. The

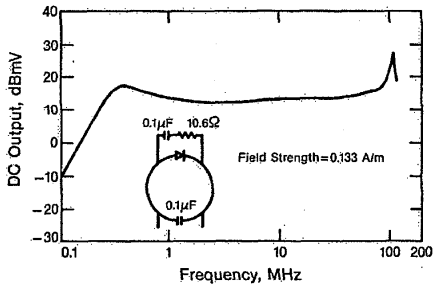

Fig. 22. Response of a compensated open-circuit-voltage loop antenna (5-turn 10-cm diam).

resonant frequency and Q of the simplified equivalent circuit are given by

$$f_0 = \frac{1}{2\pi\sqrt{C_3 - (C_3R)^2}} \tag{31}$$

and

$$Q = \frac{2\pi f_0 L_a}{R} \tag{32}$$

where C_3 is the net capacitance of the two capacitors C_1 and C_2 in series.

As an example, the response of a 5-turn compensated loop with a 10-cm diam is shown in Fig. 22. Since the inductance of a 5-turn loop with a 10-cm diam is about 7 μH, the resonant frequency is calculated from (31) to be 600 kHz, which agrees well with the experimental results.

The Q of the compensated open-circuit voltage loop is estimated to be 2.5 using (32). The resonance which occurs at about 106 MHz is the first of a series of high-frequency resonances. These resonances are found to occur when the total length of the multiturn loop is approximately equal to $\lambda/2$ or one of its multiples. In essence, to achieve a broad-band response using a compensated open-circuit voltage loop, the first resonance is shifted by adding proper capacitance of C_1 and C_2, and its Q is adjusted by the series resistor R. Using both the lowest and next lowest resonances and adjusting the Q of the first resonance, one can achieve a broad-band response of the loop antenna.

The above model assumes that the loop antenna with attached line and load are symmetrical with respect to a plane perpendicular to the loop and passing midway between its symmetrically located terminals. If the loop antenna is near a conducting surface such as the Earth, this surface must be parallel to the plane of the loop.

It is possible to achieve complete electrical symmetry for a receiving loop by enclosing it entirely in a metal shield that has a gap at the top (or at the bottom). A potential difference is maintained across the gap, almost wholly as a result of current induced in the shield. In general, a codirectional vertical current due to the electric field is also excited, but it contributes nothing to the potential difference across the gap because it charges the gap edges equally with charges of the same sign. Under these con-

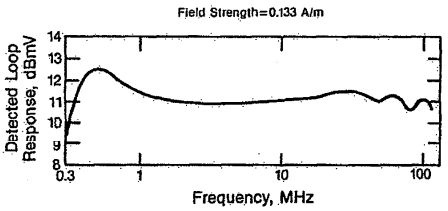

Fig. 23. Response of a compensated open-circuit-voltage loop antenna with shielding (5-turn, 10-cm diam).

ditions, loop current is excited by the induced voltage across the gap, and this is due only to the circulating current in the shield.

In general, shielding causes very little effect on the low-frequency loop response. As the frequency increases, it does, however, cause a very pronounced effect on the high-frequency loop response. The gap voltage, which is the product of the circular current and gap impedance, decreases linearly with frequency, because the gap capacitive reactance decreases linearly with frequency. Thus the current in the loop, excited by the gap-induced voltage, decreases linearly with frequency. This high-frequency filtering action smoothes out some of the undesirable effects of high-frequency resonance, as shown in Fig. 23.

The electric and magnetic field probes discussed above measure either the electric or magnetic field only, and cannot, therefore, measure complicated EM fields such as those with reactive near-field components, multipath reflections, etc. For this reason, a single sensor capable of performing simultaneous electric and magnetic field measurements was developed at NBS [34]. In this case, a loop is loaded at diametrically opposite points with equal impedances. It can be shown that across one load the magnetic-loop response adds to the electric-dipole response, whereas across the other load, the magnetic-loop response subtracts from the electric-dipole response. Thus by taking the sum and difference of currents across loads at diametrically opposite points, the magnetic-loop response and electric-dipole response can be separated. That is, the sum current gives a measure of the magnetic field, whereas the difference current gives a measure of the electric field.

To explain the basic characteristics of a doubly loaded loop, the currents I_1 and I_2 at each load are examined:

$$I_1 = 2\pi b E_0^i \left(\frac{f_0 Y_0}{1 + 2Y_0 Z_L} + \frac{f_1 Y_1}{1 + 2Y_1 Z_1} \right) \tag{33}$$

and

$$I_2 = 2\pi b E_0^i \left(\frac{f_0 Y_0}{1 + 2Y_0 Z_L} - \frac{f_1 Y_1}{1 + 2Y_1 Z_L} \right) \tag{34}$$

where b is the radius of the loop, E_0^i is the incident electric field, Z_L is the load impedance, Y_0 is the admittance for the magnetic-loop response, and Y_i is the admittance for the electric-dipole response of a loop. In general Y_0 is much larger than Y_1. f_0 and f_1 are Fourier coefficients of the incident wave. For a loop orientation of maximum electric and magnetic field response, $f_0 = j\beta b/2$ and $f_1 = 1/2$.

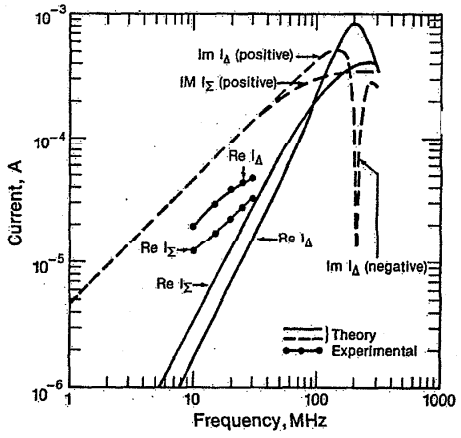

Fig. 24. Magnetic-loop (I_Σ) and electric-dipole (I_Δ) currents of a loop antenna with $Z_L = 200\ \Omega$.

Taking the sum and difference of these currents, one obtains

$$I_\Sigma \cong \frac{1}{2}(I_1 + I_2) = 2\pi b E_0^i \frac{f_0 Y_0}{1 + 2Y_0 Z_L} \tag{35}$$

and

$$I_\Delta \cong \frac{1}{2}(I_1 - I_2) = 2\pi b E_0^i \frac{f_1 Y_1}{1 + 2Y_1 Z_L}. \tag{36}$$

This indicates that the sum current can be used to measure the magnetic field and the difference current can be used to measure the electric field.

In general, $2Y_0 Z_L > 1$ for the magnetic-field loop current. Therefore, one can make the approximation

$$I_\Sigma \cong j \frac{E_0^i}{2Z_L} \pi b^2 \beta \tag{37}$$

which indicates that the magnetic-loop current is approximately proportional to the product of frequency and the area of the loop, and inversely proportional to the load impedance. Similarly, for the electric-field dipole current assuming that $2y_1 z_2 \ll 1$

$$I_\Delta \cong \pi b E_0^i Y_1 \tag{38}$$

which is approximately proportional to the product of the circumference of the loop and frequency, since Y_1 has a capacitive susceptance (positive) and increases with frequency.

The sum and difference currents in the loop with $Z_L = 200\ \Omega$, calculated using (37) and (38), are shown in Fig. 24 along with experimental results. The real parts of the currents increase with frequency up to about 200 MHz, as indicated in (37) and (38). With a load impedance of 200 Ω, the magnetic-loop current is larger than the electric-dipole current up to 100 MHz, whereas the electric-dipole current becomes larger than the magnetic-loop current above 100 MHz. This device is intended not only to measure the polarization ellipses of the electric- and magnetic-field vector in the near-field region, but hopefully also to measure the time-dependent Poynting vector and describe the energy flow.

V. Future Directions

For EM field measurements it is always likely that established techniques will be extended to other frequencies; however, such work does not involve fundamental changes in the instrumentation or measurement strategy. The measurement methods described earlier are exclusively suitable for (1) measuring plane wave sinusoidal fields of a given frequency, and (2) calibrating the devices which measure such fields.

The challenges of the future reside in the development of standards for measurement of fields which are nonsinusoidal and/or nonplanar. The fundamental requirement for field probes will be that their output must simultaneously provide amplitude and phase information, and necessarily over a broad spectrum for nonsinusoidal fields. In other words, the output of a probe would be proportional to the time variation of the field being measured. For fields containing more than one frequency component it is clear that such simultaneous measurement is necessary. Similarly, if phase information is preserved, then measurements of single-frequency nonplanar fields could be made in terms of true energy density or in terms of the Poynting vector.

The standard techniques of today rely upon very high-resistance transmission lines to convey dc voltage and current to regions external to the field under measurement. Future standards of measurement will employ optically sensed probes whose optical sensing signal paths will not perturb the EM field under measurement, but will convey field amplitude and phase information to a region external to the field for measurement. Optically sensed probes are being built today and are being studied at NBS [35]. However, much work must be done to transform these experimental devices into stable elements for standards applications. Also, there is much work to be done to develop standard fields for calibration of these probes of the future.

References

[1] M. Kanda, "A methodology for evaluating microwave anechoic chamber measurements," in *Proc. of EMC Symp.*, Swiss Federal Institute of Technology, Zurich, Switzerland, March 5–7, 1985.

[2] D. M. Kerns, "Plane-wave scattering-matrix theory of antennas and antenna-antenna interactions," Nat. Bur. Stand. (U.S.) Monogr. 162; p. 162, June 1981.

[3] J. A. Stratton, *Electromagnetic Theory.* New York: McGraw-Hill, 1941, p. 615.

[4] A. D. Yaghjian, "Approximate formulas for the far fields and gain of open-ended rectangular waveguide," Nat. Bur. Stand. (U.S.) NBSIR 83-1689, p. 34, May 1983.

[5] A. D. Yaghjian "Efficient computation of antenna coupling and fields within the near-field region," *IEEE Trans. Antennas Propagat.*, vol. AP-30, pp. 133–138, Jan. 1982.

[6] M. Kanda, "Near-zone gain calculations of open-ended waveguides and rectangular pyramidal horns for anechoic chamber measurements," to be published.

[7] S. A. Schelkunoff, *Electromagnetic Waves.* New York: Van Nostrand Reinhold, 1943, p. 530.

[8] E. V. Jull, "Errors in the predicted gain of pyramidal horns," *IEEE Trans. Antennas Propagat.*, vol. AP-21, pp. 25–31, Jan. 1973.

[9] R. G. FitzGerrell, "Using free-space transmission loss for evaluating anechoic chamber performance," *IEEE Trans. Electromagn. Compat.*, vol. EMC-24, Aug. 1982.

[10] F. M. Greene, "NBS field-strength standards and measurements (30 Hz to 1000 MHz)," *Proc. IEEE*, vol. 55, pp. 970–981, June 1967.

[11] H. E. Taggart, "Field strength and RFI standards at the National Bureau of Standards," in *Proc. 1968 IEEE Symp. on EMC*, Seattle, WA, pp. 149–158, July 1978.

[12] H. E. Taggart and J. L. Workman, "Calibration principles and procedures for field strength meters (30 Hz to 1 GHz)," Nat. Bur. of Stand., Tech. Note 370, Mar. 1969.

[13] *The Radio Frequency Interference Meter*, NAVSHIPS 94180, U.S. Navy, July 1962, p. 201.

[14] "An investigation into existing calibration methods of field intensity meters," D. R. Clark, Project Leader, RADC-TR-64-527, p. 228, Jan. 1965.

[15] F. M. Greene, "The near-zone magnetic field of a small circular-loop antenna," *J. Res. Nat. Bur. of Stand. (U.S.) C Eng. and Instr.*, vol. 71C, no. 4, Oct.–Dec. 1967.

[16] "Methods for measuring electromagnetic field strength for frequencies below 1000 MHz in radio wave propagation," *IEEE Std.*, p. 302, Aug. 1969.

[17] F. M. Greene and M. Solow, "Development of very-high-frequency field-intensity standards," *J. Res. Nat. Bur. of Stand. (U.S.)*, vol. 44, pp. 527–547, May 1950.

[18] S. A. Schelkunoff and H. T. Friis, *Antennas, Theory and Practice.* New York: Wiley, 1952, p. 306.

[19] E. C. Jordan, *Electromagnetic Waves and Radiating Systems.* New York: Prentice-Hall, 1950, pp. 323–324.

[20] M. L. Crawford, "Generation of standard EM fields using TEM transmission cells," *IEEE Trans. Electromagn. Compat.*, vol. EMC-16, pp. 189–195, Nov. 1974.

[21] M. L. Crawford, "Generation of standard EM fields for calibration of power density meters 20 kHz to 1000 MHz," Nat. Bur. Stand. (U.S.), NBSIR 75-804, Jan. 1975.

[22] J. C. Mitchell, "A radio frequency radiation exposure apparatus," Brooks Air Force Base, School of Aerospace Medicine, Tech. Rep. SAM-TR-70-43, July 1970.

[23] J. C. Tippet and D. C. Chang, "Radiation characteristics of dipole sources located inside a rectangular coaxial transmission line," Nat. Bur. Stand. (U.S.), NBSIR 75-829, Jan. 1976.

[24] T. S. Chen, "Determination of the capacitance, inductance, and characteristic impedance of rectangular lines," *IRE Trans. Microwave Theory Tech.*, vol. MTT-8, pp. 510–519, Sept. 1960.

[25] M. L. Crawford and J. L. Workman, "Using a TEM cell for EMC measurements of electronic equipment," Nat. Bur. Stand. (U.S.), Tech. Note 1013, p. 65, July 1981.

[26] M. L. Crawford, "Improving the repeatability of EM susceptibility measurements of electronic components when using TEM cells," presented at the Int. Congress Exposition, Detroit, MI, Feb. 28–March 4, 1983, and in *SAE Handbook*, 1984.

[27] J. C. Tippet, "Model characteristics of rectangular coaxial transmission line," Ph.D. dissertation, E.E. Department, University of Colorado, Boulder, June 1970.

[28] C. M. Weil, W. T. Joines, and J. B. Kinn, "Frequency range of large-scale TEM mode rectangular strip lines," *Microwave J.*, pp. 93–113, Nov. 1981.

[29] P. F. Wilson and M. T. Ma, "Small aperture analysis of the dual TEM cell and an investigation of test object scattering in a single TEM cell," Nat. Bur. Stand. (U.S.), Tech. Note 1075, Oct. 1984.

[30] M. Kanda, "Electromagnetic-field distortion due to a conducting rectangular cylinder in a transverse electromagnetic cell," *IEEE Trans. Electromagn. Compat.*, vol. EMC-24, pp. 294–301, Aug. 1982.

[31] M. Kanda, "Analytical and numerical techniques for analyzing an electrically short dipole with a nonlinear load," *IEEE Trans. Antennas Propagat.*, vol. AP-28, pp. 71–78, Jan. 1980.

[32] E. B. Larsen and F. X. Ries, "Design and calibration of the NBS isotropic electric-field monitor (EFM-5), 0.2 to 1000 MHz," Nat. Bur. Stand. (U.S.), Tech. Note 1033, p. 97, Mar. 1981.

[33] M. Kanda, F. X. Ries, L. D. Driver, and R. D. Orr, "Design considerations for broadband magnetic-field sensors," in *IEEE Digest-Conf. on Precision Electromagnetic Measurements 1982*, pp. P-11 to P-13, June 28–July 1, 1982, Boulder, CO.

[34] M. Kanda, "An electromagnetic near-field sensor for simultaneous electric and magnetic-field measurements," *IEEE Trans. Electromagn. Compat.*, vol. EMC-26, pp. 102–110, Aug. 1984.

[35] J. C. Wyss, M. Kanda, D. Melquist, and A. Ondrejka, "Optical modulator and link for broadband antennas," in *Conf. on Precision Electromagnetic Measurements*, Boulder, CO, IEEE Cat. 82 CH 1737-6, pp. P-16 to P-17, June 1982.